CLM-R231

CLM-R231

UKAEA

Report

LIQUID LITHIUM AS A COOLANT FOR TOKAMAK FUSION REACTORS

R. J. HOLROYD
J. T. D. MITCHELL

CULHAM LABORATORY
Abingdon Oxfordshire

1982

C/18 Available from H. M. Stationery Office £3.00

CLM-R 231

LIQUID LITHIUM AS A COOLANT FOR TOKAMAK FUSION REACTORS

R.J. Holroyd*, J.T.D. Mitchell
Culham Laboratory, Abingdon, Oxon, OX14 3DB, UK
(Euratom/UKAEA Fusion Association)

Abstract

Three-dimensional magnetohydrodynamic flows due to streamwise variations of duct dimensions and shape and magnetic field strength produce pressure gradients larger than those predicted by assuming local fully developed flow. These effects are included in this study of lithium cooling of the blanket of the Culham Conceptual Tokamak Reactor Mark IIA.

Principal results are summarised in terms of the pumping power required to circulate the lithium coolant for specific wall loadings for various coolant piping designs and ranges of operating parameters. Three ducting arrangements are considered and the best performance is achieved by adopting an innovatory concept in which the ducting is incorporated into the tritium breeding section of the blanket and a second low pressure lithium flow circuit is used for that part of the blanket in the lower magnetic fields on the outer side of the torus. The calculated maximum wall loading is about 6 MW/m^2 for a pumping power fraction of 2.5% of the reactor thermal output. The results neglect any necessary reduction of working stress of the blanket structural materials due to radiation damage and cyclic loadings because of the inadequacy of presently available materials data.

* Oxford, consultant

November 1982

ISBN 0 85311 115 4

* Oxford, consultant

November 1982

ISBN 0 85311 115 4

CONTENTS

1. Introduction

Lithium is one of several possible coolants being considered for the blanket of magnetic confinement toroidal fusion reactors, not only because of its good thermal and neutron moderating properties, but also because calculations have shown that the tritium required to fuel the reactors can be produced by neutron reactions in the lithium. Against these qualities is the fact that the power required to circulate the lithium may be unacceptably high. By virtue of being an electrical conductor flowing in a region of magnetic field, electric currents are induced in the lithium fluid which interact with the magnetic field giving rise to forces which affect the motion and, in general, create pressure gradients much larger than in hydrodynamic flows. Any study of liquid metal coolant flow must be based, therefore, on a sound understanding of magnetohydrodynamics (MHD). Unfortunately, this is not a feature of some contemporary reports on this problem and consequently their findings may be over-optimistic.

In 1970 the MHD pressure losses in a lithium cooled fusion reactor were reported by Hunt and Hancox (1). This report is a fresh appraisal of that basically same problem but viewed in the light of the significant advances made in both reactor design and MHD during the past decade. Furthermore, it also complements the recent study by Shock (2) of helium cooling of a fusion reactor. In addition, it is hoped that it will demonstrate the application of modern MHD studies to the practical problems of liquid metal flow in a magnetic field.

Inevitably, in a report of this nature, it is not possible to do a complete study of a lithium cooled reactor. Instead, necessary parts of the reactor's structure are taken as given constraints and the blanket and pipes required for the cooling circuit are fitted into the available space leaving a fraction of that space for

thermal insulation and supporting structure. Only that part of the flow circuit within the toroidal field coils is considered - heat exchangers and pipework in the external circuit are accounted for by a small pressure drop.

2. The Reactor

In this report the lithium coolant flow in the Culham Conceptual Tokamak Reactor Mark IIA is considered. The reactor is illustrated in Fig. 1 and described by Mitchell and Hollis (3). So far as the study of the lithium flow is concerned only half of one of the 20 wedge-shaped segments between adjacent magnetic field coils of the torus need be considered because of their symmetric form about the mid-plane. A typical half-segment is shown in Fig. 2 together with the radial variation in strength of the toroidal magnetic field. At present it is envisaged that all parts of the flow circuit and attendant structure will be made of stainless steel.

Energy transfer to the lithium, along with the consequent breeding of tritium, takes place in the blanket comprising numerous cells packed around the periphery of the segment, a concept discussed by Mitchell and Hancox (4), while the detailed construction of such cells is examined by Stanbridge et al (5). To provide an adequate tritium breeding ratio in the blanket, the structure volume fraction - defined as the ratio of the volume of material making up the cells to the volume of space enclosed by those cells - must be small, say 0.06 - 0.07. When this criterion and several others are considered, suitable cell dimensions, quoted by Mitchell and Hancox, are

Maximum mean diameter - 0.3m
Length - 0.6m with a further 0.25m of graphite or stainless steel reflector
Wall thickness - 4.5mm

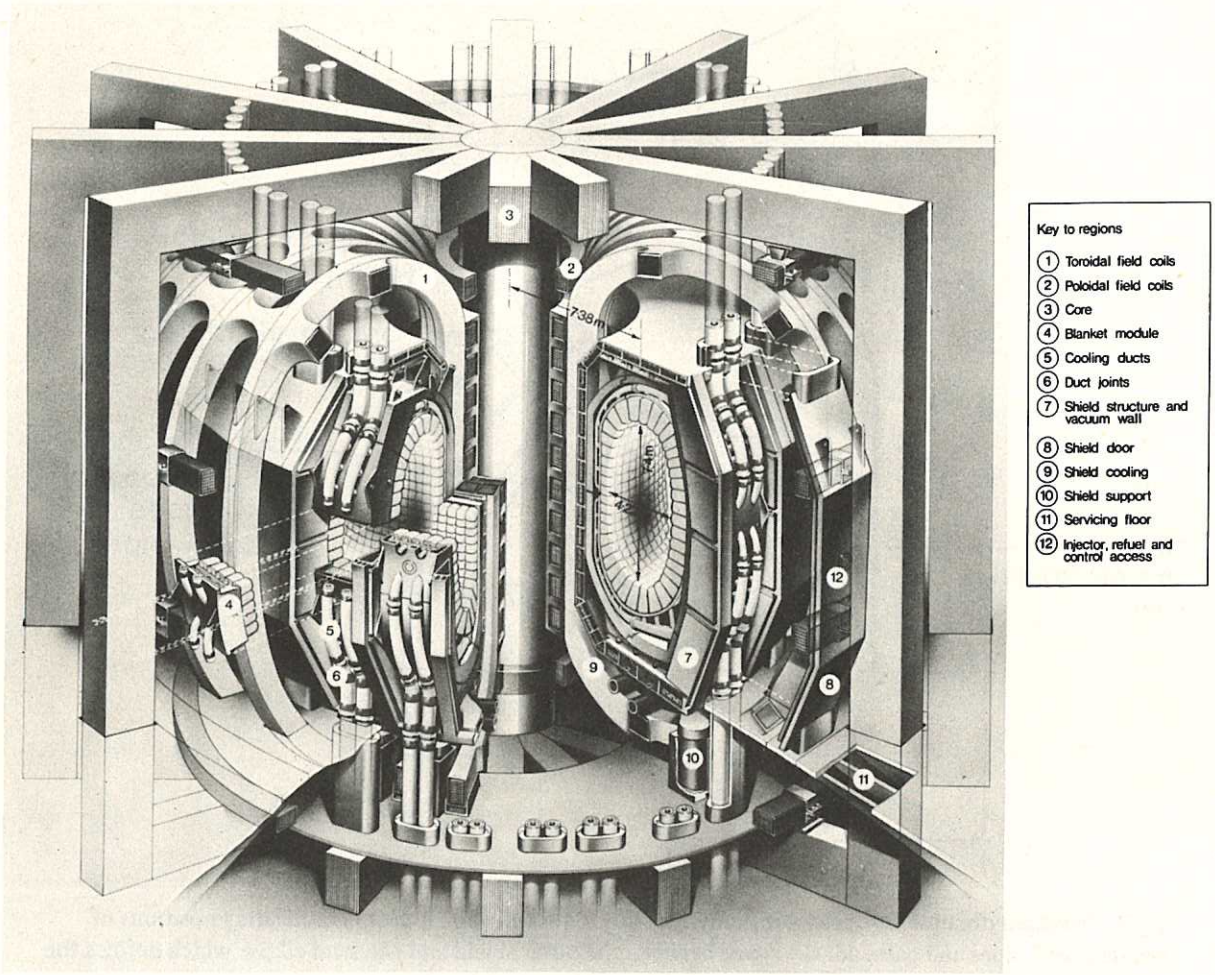

Culham Conceptual Tokamak Reactor Mk II

Fig.1 Artist's impression of the Culham Conceptual Tokamak Reactor Mark IIA. In this case the primary feed pipes are aligned vertically and each divides into two single secondary feed pipes following the minor circumference of the torus to the narrow and wide parts of a half segment.

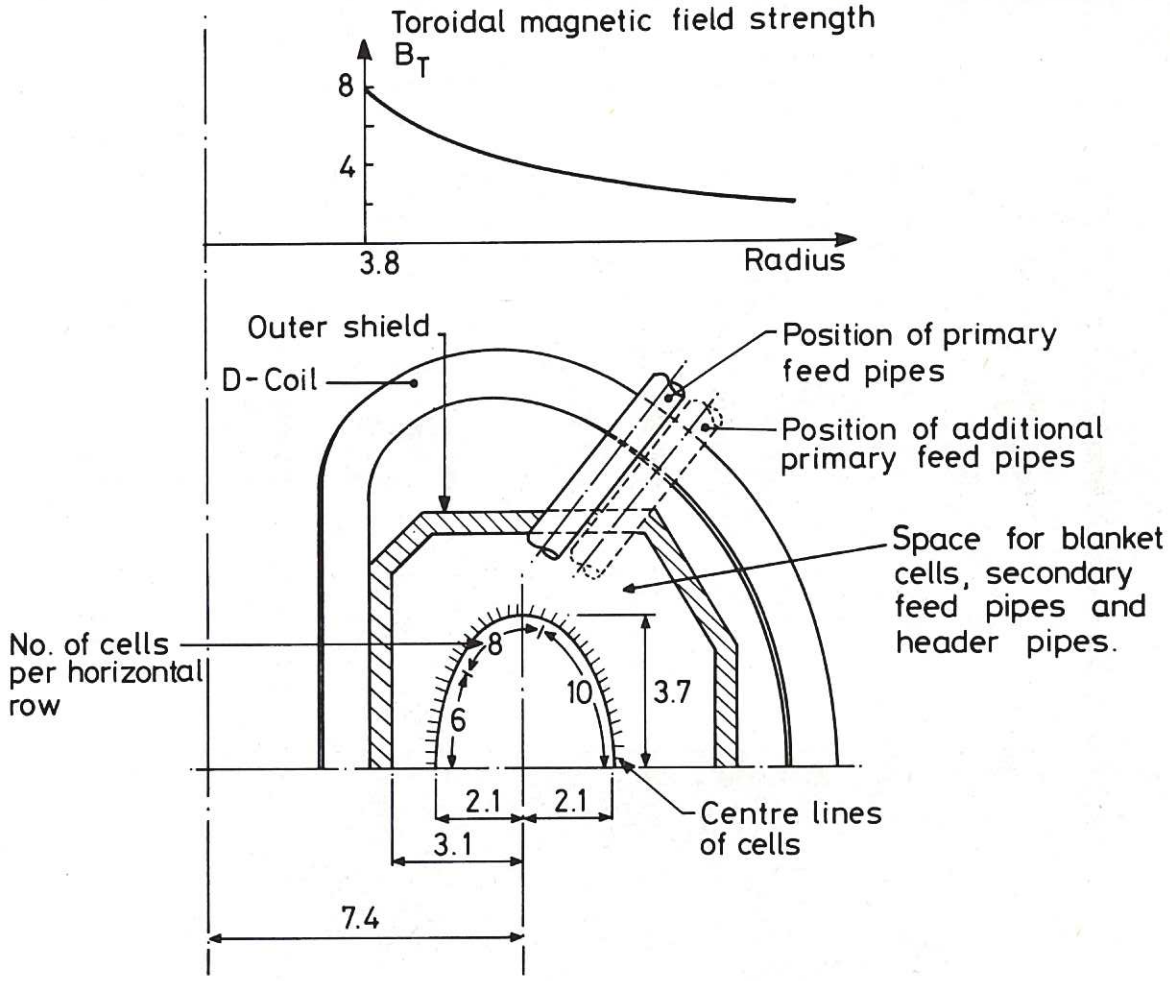

Fig.2 Principal dimensions of reactor in metres (from Mitchell and Hollis (3)) indicating positions of primary feed pipes and cells. All the space between the outer shield and the semi-ellipse which defines the envelope of the front faces of the cells is available for blanket and supply pipework. Above is shown the radial variation of the toroidal magnetic field strength.

For a simple cell model with a flat end, these dimensions yield a structure fraction of 0.0675 when the volume of any internal structural fittings is neglected (note that for such cells Mitchell and Hancox quote a slightly smaller value of 0.060). However, while it is possible to adhere to the latter two dimensions, the shape of the inside surface of the segment means that the radius of each cell will depend on its position on that surface. Here, a distribution of six cells per horizontal row on the inside (narrow side) of the segment increasing to eight over the central section and finally ten on the outside (see Fig. 2) has been chosen to satisfy the maximum cell diameter criterion and this arrangement has a structure fraction of 0.072.

Assuming that the incident energy per unit area is uniform over the front surface of the cells, then the amount of coolant supplied to each cell must be proportional to the area of its end face.

The immediate link between the cells and the external flow circuit are two primary feed pipes (inlet and outlet). These divide into secondary feed pipes which follow the minor circumference of the torus and feed the cells either directly or via header pipes running horizontally around the major circumference of the torus. All this pipework must fit into the space between the rear of the cells, the outer shield and the 'sides' of the segment. To allow space for supporting structure, thermal lagging, assembly, maintenance etc, the outside diameter of each pipe is taken as 80% of the value dictated by spatial considerations. With the exception of the principal feed pipes, Shock (2) did not mention this point although the dimensions of his pipes are similar to those derived here.

The thermal performance of the coolant system is governed by the temperature rise and maximum temperature of the lithium. Here the inlet temperature of the lithium is

taken as 250°C (64°C above its melting point). There are no strong reasons for selecting this value - Stanbridge et al (5) for example use 286°C. On the other hand, the outlet temperature is governed by the limitations of the pipe and cell materials, particularly corrosion and creep effects, and the life expectancy of the pipework and cells. Stanbridge et al (5) base their calculations on a temperature maximum of 500°C at the lithium/stainless steel interface for an acceptable corrosion rate. However, it now appears that creep is a more important factor and in view of this a maximum mean steel temperature of 475°C is employed here.

The pressure in the outlet primary feed pipe where it crosses the field coils is determined by the flow in the circuit outside the field coils. Obviously this pressure will increase as the flow rate increases but without any firm details of the external circuit it is not possible to specify a relationship between the two quantities. Stanbridge et al (5) used a linear relationship between pressure and energy deposition in the blanket but here a fixed value of 0.3 MN/m^2 has been chosen, which Mitchell and Hancox (4) regard as suitable for wall loadings of about 4 MW/m^2.

3. MHD Considerations

3.1 Pipes normal to the magnetic field

In hydrodynamics the pressure gradient in an either laminar or turbulent pipe flow is a function of only the Reynolds number and resistance to motion can be traced back to viscosity. In MHD the fluid motion is principally opposed by an electromagnetic force created by the interaction of electric currents flowing in the liquid conductor and the magnetic field where the currents are themselves generated by interaction of the motion of the fluid and the magnetic field. Now the pressure gradient of

the usually laminar flow (in marked contrast to hydrodynamic flows) depends upon three parameters, namely

Hartmann number	$M = aB\sqrt{\sigma/\eta}$
Interaction parameter	$N = M^2/Re = \pi\sigma a^3 B^2/Q$
Conductance ratio	$\Phi = \sigma_w t/\sigma a$

where B = magnetic field strength, Q = local mass flow rate of liquid, a = inside radius of pipe, t = wall thickness of pipe, σ_w = electrical conductivity of pipe wall, σ = conductivity of liquid, η = viscosity of liquid and $Re = Q/\pi\eta a$ = Reynolds number. (Usually N and Re are defined in terms of the mean flow velocity but here the mass flow rate is used; consistency with the usual definitions is achieved by including the factor π.) For lithium at 400°C flowing at 0.3 kg/s along a stainless steel pipe of 0.1m diameter and 1mm thick wall in a field of 6 T, $M \sim 27000$, $N \sim 145000$, $Re \sim 5000$ and $\Phi \sim 0.0085$ (values such as these occur near the end of a secondary feed pipe on the narrow side of the segment).

Recent advances in MHD theory have been for such values of these parameters, more generally, high M, high N and low Φ and so there is now a large corpus of theoretical results upon which pressure loss and heat transfer estimates can be based. Laboratory experiments designed to test the theoretical results are hampered by the fact that high values of M and N are difficult to attain. Indeed, it can be said that there are no reliable experimental results for values of M and N in excess of 1000. Nevertheless, what results there are support the general features predicted by theoretical work. A review by Hunt and Holroyd (6) summarises the recent work in both theoretical and experimental MHD research, and its relationship to fusion reactor design problems.

Not unexpectedly, if the flow is in a pipe of varying cross-section and/or in a principally transverse magnetic

field of spatially varying strength then the flow structure is three-dimensional and the pressure distribution is non-linear.

When such changes as these are confined to a short length of the pipe system (e.g. two pipes of different radii connected by a conical diffuser of cone angle, say, 45^{o}), the pressure distribution can be regarded as being that of fully-developed flow (i.e the two-dimensional flow in a uniform bore pipe in a uniform magnetic field) in which the pressure gradient is constant in each pipe together with a large pressure drop at the junction. This has been predicted theoretically (Holroyd and Walker (7)) and verified in experiments (Holroyd (8)). That theory also predicts that the internal structure of the flow will be three-dimensional around the junction with the fully-developed flows only being realised at distances of about $a\Phi^{-\frac{1}{2}}$ both upstream and downstream of the junction. However, at present there is no experimental confirmation of this.

On the other hand, when the changes are spread out over a substantial length of the pipe (e.g. in the aforementioned diffuser example, the cone angle is decreased to about $\mathrm{Tan}^{-1}\ \Phi^{\frac{1}{2}}$) the flow may be regarded as being locally fully-developed throughout - i.e. there is no additional pressure drop due to the change of diameter over the conical section (Holroyd (9, section 9.3 and Fig. 12.2)).

The coolant circuit will comprise a number of interconnected straight, uniform bore pipe segments most of which will be at right angles to the lines of a spatially varying magnetic field (see Fig. 2). Thus, for any pipe segment of length ℓ, the pressure drop across it will comprise a contribution from the fully-developed flow pressure drop Δp_1 and another from the finite pressure drop Δp_2 associated with the junction and field strength variation. The former may be calculated from the theory of

Chang and Lundgren (10) as

$$\Delta p_1 = p_{in} - p_{out} = \frac{\sigma Q B^2 \ell}{\pi a^2 \rho} \cdot \frac{\Phi}{1 + \Phi} \qquad (1)$$

(ρ = density of fluid). A value for Δp_2 is not easily specified. For the case of a straight tube situated in two adjacent transverse magnetic fields of strengths, B and B' (< B) theory shows that Δp_2 varies with the ratio B'/B with a peak value of $0.16\Phi^{\frac{1}{2}}\sigma Q B^2/\pi a \rho$ (Holroyd and Walker (7)). Complementary experimental values for B'/B = 0.5, M = 500, 13 < N < 50 indicate a value almost double this. Here a value of

$$\Delta p_2 = 0.2\Phi^{\frac{1}{2}}\sigma Q B^2/\pi a \rho \qquad (2)$$

has been used wherever necessary.

A first important implication of equations (1) and (2) is that both pressure drops vary directly with the thickness of the tube wall t, through Φ . Therefore t must be as small as possible to minimise the pressure drop but at the same time it must be large enough to withstand the internal pressure in the pipe. Here it will be assumed that the effects of longitudinal and radial stresses and strains can be neglected so that the pressure p is related to the working stress f of the tube wall material and its wall thickness t through the Lamé hoop stress equation.

$$p/f = \{(a + t)^2 - a^2\}/\{(a + t)^2 + a^2\} \qquad (3)$$

Thus the minimum pressure drop along the pipe segment is achieved by having a pipe wall thickness given by combining equations (1), (2) and (3) as

$$p_{out} + \Delta p_1 + \Delta p_2 = f\{(a + t)^2 - a^2\}/\{(a + t)^2 + a^2\} \qquad (4)$$

In practice the feed pipe comprises two co-axial cylinders joined only at the nose end which has the desirable effect of insulating the fluid it contains from that in the cell both electrically and thermally as well as reducing stresses due to differential thermal expansion (Carruthers (12, Sec 4.3.6)). Therefore the flow structure in the cell will be similar to that in two pipes of different radii joined together except that the smaller pipe is inside the larger and the flows are in opposite directions. Probable streamlines are sketched in Fig. 3. A notable feature of the flow is the pair of trapped co-rotating eddies which extend along the cell for a distance of about $a_f\Phi^{-\frac{1}{2}}$. Because of the relatively high conductance of the solid reflector ($\Phi \geqslant 0.3$) there is probably much less distortion of the flow immediately ahead of it with the streamlines diverging as shown.

An estimate of the pressure drop across the cell comprises several parts which, following the flow backwards, are

(i) contraction as flow past reflector converges on cell outlet pipe whose radius is taken to be the same as cell feed pipe - apply equation (2) with Φ based on outlet pipe dimensions

(ii) annulus of length L_a formed by cell body and reflector - using the expression quoted by Holroyd and Hunt (11, Sec 6.2) and assuming the reflector to have a high conductivity and a radius of $0.95a_c$ then

$$\delta p = 0.005\sigma Q B^2 L_a / \rho\pi\{a_c^2 - (0.95a_c)^2\}$$

(iii) expansion from annulus specified in (ii) to annulus formed by cell body and feed pipe - apply equation (2) with Φ (= 0.012) based on the cell body dimensions so that

$$\delta p = 0.2\phi^{\frac{1}{2}}\sigma Q B^2 a_c/\rho\pi(a_c^2 - a_f^2)$$

(iv) annulus formed by cell body and feed pipe - applying the expression used in (ii) yields

$$\delta p = 0.0155\sigma Q B^2 L/\rho\pi(a_c^2 - a_f^2)$$

(v) shear layer at mouth of feed pipe. Experiments designed to determine this pressure drop are reported by Holroyd and Hunt (11, Sec 6.2). Results for M = 150, N $\leqslant$ 30 and Φ = 0.12 (based on feed pipe dimensions) suggest that for a given t_f the pressure drop tends to an asymptotic value as N $\to \infty$ while for N = 9.64 the pressure drop tends to nearly the same value as $t_f \to \infty$. Although there is no evidence to support the view, it will be assumed that the pressure drop varies with $\Phi^{\frac{1}{2}}$ in common with the pressure drop defined in equation (2) and so the following expression, derived from Holroyd and Hunt's results, will be used to calculate this pressure drop, namely

$$\delta p = (1.256 + 0.000135 t_f^{-1.5})\sigma Q B^2 \Phi^{\frac{1}{2}}/\rho\pi a_f$$

(vi) along feed pipe - equation (1) applies with the wall thickness of the feed pipe used to calculate Φ derived by use of equation (4) with Δp_2 set to zero.

In addition, there are further pressure drops due to the bends between the cell inlet and outlet pipes and the secondary feed pipes. If the former connect directly to the latter then there are two extra pressure drops each given by equation (2) but if there is a header pipe between them then there are four extra pressure drops which are deduced from equation (5).

4. Heat Transfer Considerations

The reflector ensures that virtually all absorption of energy from the plasma occurs within the cells and so the thermal performance of the reactor is governed by that of a cell. Of principal concern is the temperature rise of the lithium as it passes through a cell and this is determined by the maximum permissible mean temperature of the steel wall of the cell (see Sec. 2). This was last looked at in great detail by Stanbridge et al (5) and their analysis is used as a basis for the present study. However, modifications are necessary because of some different details of cell and reactor design and more realistic assumptions about the fusion reactions in the blanket.

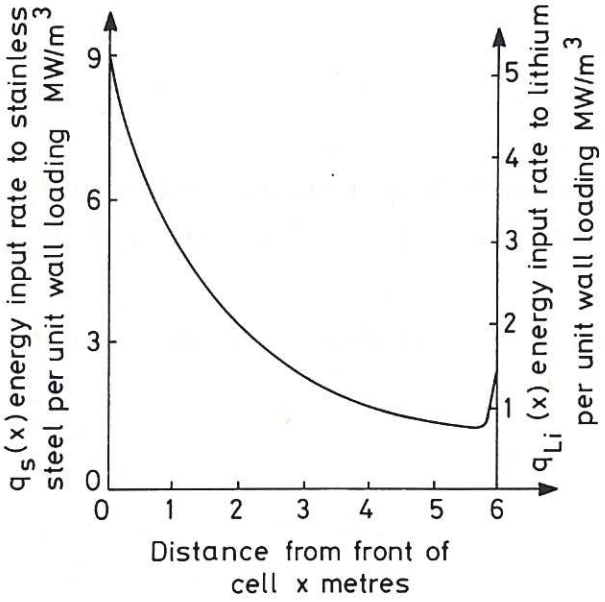

Fig.4 Variation of neutron energy input rates to stainless steel and lithium per unit wall loading with distance from front of cell.

This latter point is discussed in Appendix I, the outcome of which is Fig. 4 which shows for unit wall loading the variation of (neutron) energy input rates to lithium ($q_{Li}(x)$) and stainless steel ($q_s(x)$) with x, the distance from the nose of the cell. Here, the wall loading is defined as

$$P_w = \frac{\text{total reactor thermal output}}{\text{nominal first wall area}}$$

and it therefore includes all the energy output from the plasma even though some of the α-particle energy is not deposited in the blanket.

It is assumed here that the reactor incorporates a divertor to exhaust ash and impurities and lengthen the burn time. In addition, it is also assumed that two-thirds of the α-particle energy is carried to this divertor leaving the remainder to be deposited on the first wall through radiation and conduction loss from the plasma. Thus, the temperature of the coolant is raised only by a fraction β of the wall loading. Using the data given in Appendix I, the value of β is given as (20 - 0.67 x 3.5)/20 = 0.833.

After considering the temperatures of the lithium and stainless steel at various points of the cell, it appears that the highest steel temperature is at the rear of the cell near the front face of the reflector. Thus, the bulk lithium temperature there is the allowable mean temperature of the steel wall (T_s = 475°C) less half of the temperature drop across the wall given by

$$\Delta T_w = P_w q_s(L) t_c^2 / 2k_s$$

less the temperature drop across the lithium boundary layer given by

$$\Delta T_{bl} = P_w q_s(L) t_c a_c / 2.53 k_{Li}$$

where k_s and k_{Li} are the respective thermal conductivities of stainless steel and lithium. (This last expression depends on the Nusselt number. Stanbridge et al (5) used the value associated with a parabolic velocity profile for a laminar hydrodynamic flow. Although the streamlines shown in Fig. 3 imply a velocity profile with a minimum at the axis of the cell immediately upstream of the reflector, for the present calculations a uniform velocity profile will be assumed. Then, by following the analysis set out

in Rogers and Mayhew ((13), p.409) for example, it can be shown that the appropriate value of Nusselt number when based on a_c is 2.53.) However, with a less efficient divertor, the temperature gradients set up in the front wall of the cell to transfer to the coolant the greater α-particle energy incident on it along with the neutron energy deposited in it might be great enough for the highest steel temperature to be attained on that wall somewhere near its junction with the circular wall of the cell body. This possibility would become more likely at high wall loadings and also if the front wall of the cell was thickened.

The temperature rise of the lithium as it passes through the cell is given by

$$\Delta T_c = \beta P_w A_c / c_p Q \quad (7)$$

where c_p is the specific heat of the lithium, Q now represents the mass flow rate through one cell and A_c represents the effective cross-sectional area of the cell taken to be the area of the circumscribed regular hexagon ($2\sqrt{3}a_c^2$). This definition of A_c is used to account for the energy which is not incident on the cell nose but falls in the spaces between the cells and is assumed to be reflected into the cell body.

From these results, the wall loading/cell flow rate relationship may be deduced from the equation

$$T_s - T_{Li}(\text{inlet}) = P_w \left\{ \frac{\beta A_c}{c_p Q} + \frac{q_s(L) t_c a_c}{2.53 k_{Li}} + \frac{q_s(L) t_c^2}{4 k_s} \right\} \quad (8)$$

where $T_{Li}(\text{inlet})$ is the inlet temperature of the lithium. For the cell dimensions quoted in section 2 and using suitable values for c_p, k_{Li} and k_s, the relative magnitudes of the three terms on the right hand side of equation (8) are in the ratio $2.4/Q : 2.5 : 1$.

There are two important implications of equation (8).

One, derived by reference to equation (7), is that the temperature rise of the coolant decreases directly as P_w increases. The other is that a maximum value of P_w is reached when $Q \to \infty$. At the same time, the temperature rise of the lithium approaches zero. In physical terms this limiting state is reached when the energy output from the plasma is so large that the temperature drops represented by the last two terms on the right hand side of equation (8) attain the value of $T_s - T_{Li}(\text{inlet})$. Then an extremely high flow rate of coolant with a corresponding extremely low temperature rise is required to remove the energy.

5. Feed Pipe Layouts and Minimisation of Pressure Losses

5.1 Introduction

In Sec. 3.1 it was pointed out that the highest pressure losses would occur when pumping coolant to the narrow side of a reactor segment. More precisely, the total pressure loss is governed by the last row of cells fed by the secondary feed pipes and consequently the pipe layouts must be such as to minimise this. On moving towards the top of the segment, the pressure drop across each row of cells will be larger than that required to circulate the coolant through those cells and so flow restrictors will be necessary to control the flow rate. Such restrictors are a necessary evil, being passive elements that absorb pumping power.

In the following sections, feed pipe layouts are examined in detail beginning with the primary feed pipes (Sec. 5.2) and then three possible types of secondary feed pipe systems (Sec. 5.3). While current designs of the reactor envisage a pair of primary feed pipes (i.e. one inlet, one outlet) per half-segment, the results of this study indicate that there are significant advantages to be had by having two pairs, one pair feeding the narrow part of the segment and the other the remainder. This arrangement is described in Sec. 5.4.

The efficiency of any feed pipe layout can be

quantified in terms of the pressure drop needed to pump the coolant through the blanket at a specified flow rate. However, each layout is also subject to a qualitative criterion, namely the ease with which various parts of the reactor can be serviced, (Mitchell and Hollis (3), Mitchell (14)). Essentially, a major servicing operation calls for the removal of either a half or a whole segment (Briars and Stanbridge (15)) which in turn means that some of the feed pipes will have to be severed and subsequently reconnected (Briars and Stanbridge (16)). While the piping systems described below do not present any significant problems in this respect, clearly if four rather than two primary feed pipes are employed then segment servicing will take up more time thereby offsetting some of the advantages gained by using four pipes.

5.2 Primary feed pipes

As a first step towards the goal of minimising the pressure losses, the optimum position for the primary feed pipe/secondary feed pipe(s) junction is required. In the helium cooled reactor study by Shock (2) the axes of the primary feed pipes were vertical and in the wider side of the segment. Here it is assumed that these pipes cross the field coils at the same position as in Shock's case but their orientation is altered. As the position of their junction with the secondary feed pipes is moved towards the narrow side of the segment, the pressure drop across the narrow side decreases because there is less coolant to be pumped to that side and the flow circuit is shorter and there is corresponding increase in the pressure drop across the wide side of the segment. At the same time the length of the primary feed pipe increases, its diameter decreases slightly, the average value of the magnetic field strength increases - consequently the pressure drop along it increases. When all these facts are taken into account, the optimum position for the junction is at the top of the segment, as illustrated in Fig. 5, in which position 43% of the coolant flows to the narrow side. Unfortunately, the

pressure losses on the narrow side of the segment are larger than those on the wide side and to achieve the correct balance of flows from a single coolant supply a flow restrictor will be required in the secondary feed pipes to the wide part of the segment. Thus, the total coolant pumping power is calculated using the overall pressure drop in the primary and secondary feed pipes and cells of the narrow part of the blanket segment.

5.3 Secondary feed pipe systems

Initially two secondary feed pipe systems were studied -

I. two small bore pipes per minor circumferential cell row (see Fig. 5a)

II. two pipes whose diameters vary as they follow the minor circumference of the toroid feeding each horizontal cell row via header pipes (see Fig. 5b).

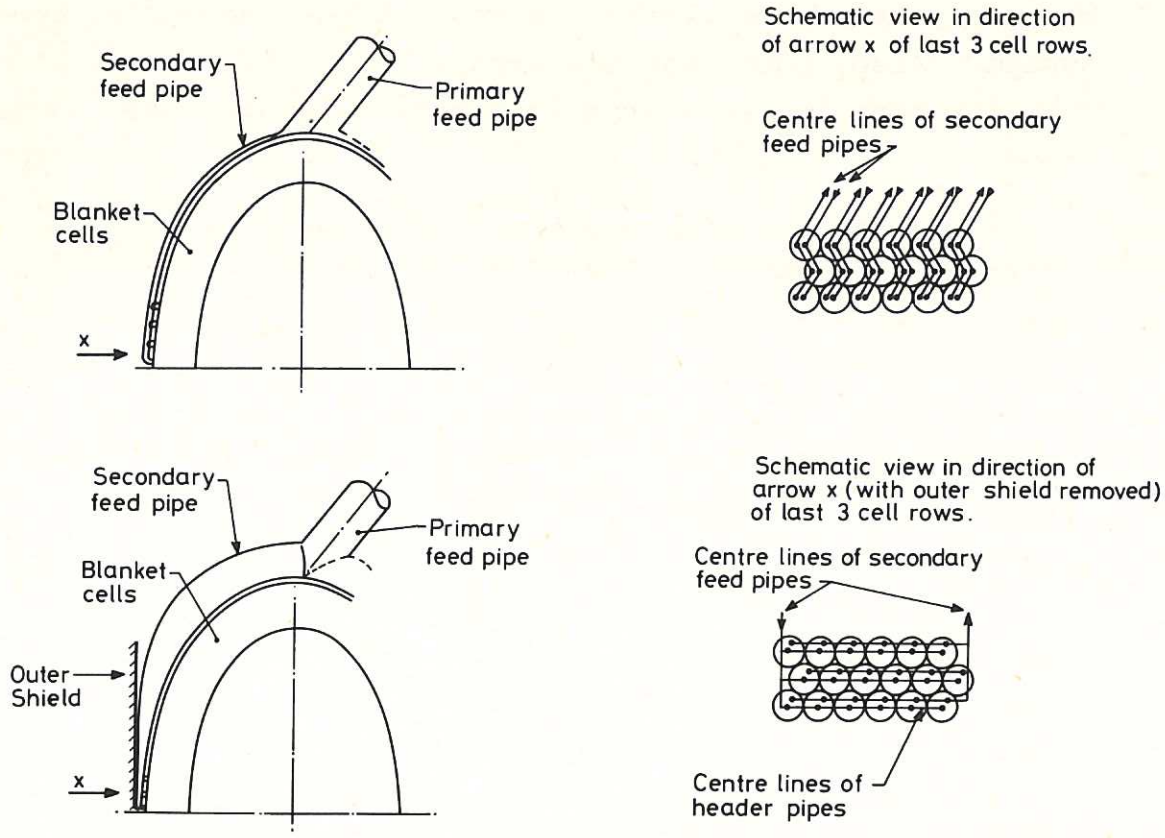

Fig.5 Arrangement of secondary feed pipes for systems I (a, top) and II (b , bottom).

Of the two systems, system II proves to have the lower pumping power requirements but it has the drawback of requiring a large volume of lithium in the secondary feed pipes, which, because it is behind the reflector, is redundant as far as heat transfer and neutronic performance is concerned.

On the basis of these facts, piping system III was evolved employing four large bore pipes feeding somewhat shorter cells of various lengths (0.45m on the inside of the segment down to 0.3m at the top) via header pipes. In particular, for any horizontal row of cells it was arranged that the longitudinal cross-sectional area of those cells together with that of the pipes behind them was the same as the area of the 0.6m long cells used in systems I and II while the outside diameter of the four pipes ensured that they filled the width of the segment at that level. The reflector is now placed between these large bore pipes and the outer shield so that the lithium contained in them becomes part of the blanket as well as the energy transport system. Also, note that the structure fraction now contains contributions from both the cells and the feed pipes.

There is, however, a problem associated with this system at the last few rows of cells. At a secondary feed pipe/header pipe junction, the flow in the former is confined initially to a shear layer whose thickness is of the order $aN^{-1/3}$ which gradually thickens over a distance of about $a\Phi^{-\frac{1}{2}}$ along the pipe, eventually filling the whole cross-section. Therefore, at the last row of cells there would be a large volume of stagnant lithium at the end of the secondary feed pipe which would lead to unacceptably high steel temperatures due to the energy deposited there which could not be removed readily. Once a mean flow is established in the secondary feed pipe this problem no longer exists and so to overcome this problem the arrangement shown in Fig. 6 is adopted; longer cells containing reflector are employed - in particular, the last cell row is basically the same as in other systems. The

secondary pipe takes on a conical form with the taper being spread over a distance of order $a\Phi^{-\frac{1}{2}}$ to minimise flow distortion (see Sec 3.1). Thereafter the short cells are used.

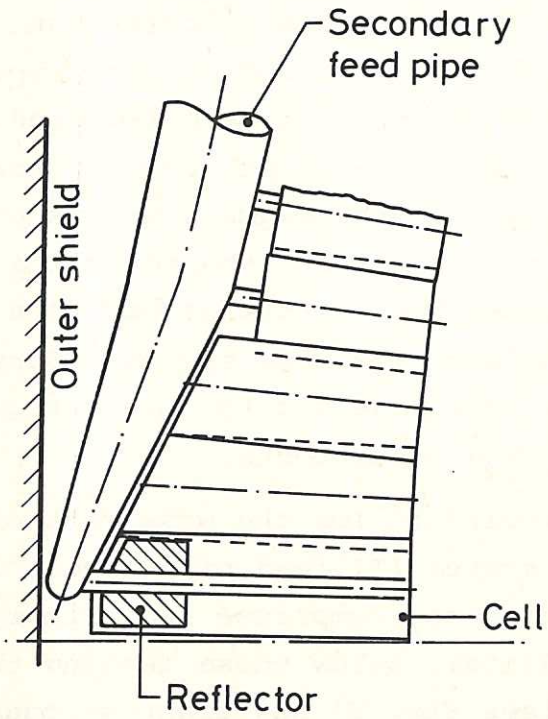

Fig.6 Modification to last three cell rows for system III and for wide part of the segment. Although not shown, the two rows of cells immediately above the last one might contain some reflector.

So far as the heat transfer in the last row of cells is concerned the analysis of Sec. 4 still applies but the absence of reflector in the remaining cells means that there will be temperature gradients along the secondary feed pipes. However, since the coolant flow to each cell is still proportional to the area of its end face then the temperature rise of the coolant across any row of cells will be the same. In Appendix II it is shown that the temperature rise of the lithium along the inlet secondary feed pipe is $0.00618\ P_w/c_p Q\ ^{o}C$ and this must be added to the right hand side of equation (8).

5.4 A separate flow circuit for the wide part of the segment

So far it has been assumed that the primary feed pipe carry the flow for the whole half of the segment although so far as the pressure loss calculations are concerned a specific layout of the secondary feed pipes in the wide part of the segment has not been required. However, in order to gain some idea of the pumping power requirements for the wide part of the segment when supplied from its own pair of primary feed pipes, the following feed pipe system has been modelled but no attempt has been made to find out if this is the best possible system. Furthermore, no allowance has been made for the space required for neutral beam injector and other ports.

The flow circuit for the wide part of the segment is based on the system III feed pipe layout described in the preceding action and comprises two primary feed pipes located immediately below those feeding the narrow part of the segment (see Fig. 2) and eight secondary feed pipes (four inlet, four outlet) delivering fluid to short cells (0.39m long at the top part of the segment - 0.2m long at the outside). The pipe radii and cell lengths are calculated from the algorithm used to calculate those quantities for the narrow part of the segment. For the reasons given in Sec. 5.3 this piping system is also modified to that shown in Fig. 6 for the last three cell rows. In addition, the rise in the temperature of the coolant as it flows along an inlet secondary feed pipe is now given by $0.00955\ P_w/c_pQ\ ^oC$ (see Appendix II).

It will be appreciated that a separate low pressure lithium circulating system is required i.e. with duplicate manifolds, pumps, controls and possibly additional heat exchangers.

6. Calculations and Results

The main aim of the calculations is to determine, for given wall loadings, the pumping power fraction, K, defined

as the fraction of the thermal power output of the reactor required to circulate the lithium. More specifically

$$K = \frac{\text{pressure drop across flow circuit}}{\overline{\rho} \times c_p \times \text{temperature rise of lithium}} \qquad (9)$$

where $\overline{\rho}$ is the mean density of the lithium in the flow circuit.

The sequence of events followed in calculating the required results is as follows -

(i) find P_w for the selected cell mass flow rate Q from equation (8)

(ii) find temperature rise of lithium and hence maximum lithium temperature from equation (7)

(iii) starting at outlet end of circuit (where pressure is specified) and working through circuit in opposite direction to flow, calculate pressure drop across and wall thickness of each length of pipe in turn using equations (1-4) until cell is reached. For systems I and II evaluate physical properties at maximum lithium temperature. For system III allow for small temperature increase between outlet and cell as outlined in Sec. 5.3

(iv) calculate t_f from equation (6)

(v) calculate pressure drop across cell, as described in Sec. 3.3

(vi) starting at inlet to cell, repeat pressure drop calculations described in (iii) until inlet to flow circuit reached. For systems I and II evaluate physical properties at lithium inlet temperature. For system III allow for small temperature decrease between cell and inlet to circuit.

(vii) calculate pumping power fraction, K, from equation (9).

Details of the variation in the principal properties of lithium with temperature are from Monstellar et al (17) while the working stress/temperature and electrical

conductivity/temperature relationships for stainless steel shown in Fig. 7 are given by Shock (2, Fig. 5) and by Kaye and Laby (18) respectively. Note that the former is for

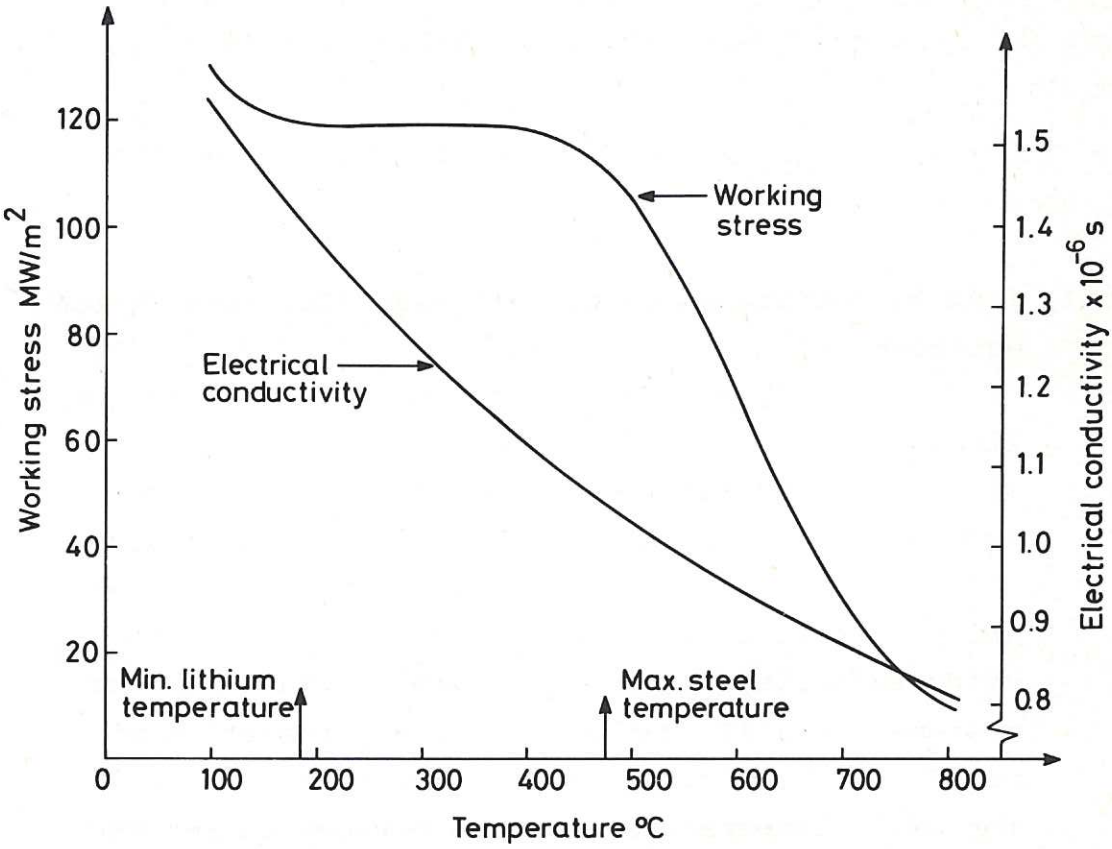

Fig.7 Variation of working stress (unirradiated material at constant strain) and electrical conductivity of stainless steel with temperature.

unirradiated steel at constant strain. Table I lists the duct length, radius, fraction of total flow rate and field strength for each section of the flow circuits for systems I, II, III and for the wide part of the segment.

To appreciate the significance and implications of the results of the calculations which are summarised in Figs. 8 to 13, it is necessary to consider the ideal values of some of the parameters that characterize the performance of the

Table I - Details of coolant piping systems

In each system the first line refers to the primary feed pipes. The remaining lines of figures refer to each component of the secondary feed pipes starting from the primary/secondary feed pipe junction.

Field Strength T	Pipe Length m	Pipe Radius m	Flow Rate Fraction	Field Strength T	Pipe Length m	Pipe Radius m	Flow Rate Fraction
	System I				System II		
3.52	4.60	0.465	0.432	3.52	4.60	0.465	0.432
4.27	0.486	0.0538	0.055	4.31	0.440	0.368	0.376
4.51	0.427	0.0511	0.052	4.62	0.440	0.368	0.352
4.76	0.388	0.0485	0.049	4.94	0.440	0.368	0.328
5.00	0.348	0.0463	0.046	5.21	0.400	0.356	0.307
5.23	0.308	0.0446	0.044	5.49	0.360	0.340	0.286
5.42	0.277	0.0431	0.041	5.71	0.330	0.329	0.267
5.60	0.266	0.0418	0.039	5.90	0.300	0.317	0.248
5.76	0.255	0.0407	0.037	6.10	0.280	0.308	0.231
5.91	0.245	0.0397	0.035	6.27	0.250	0.300	0.213
6.08	0.317	0.0515	0.033	6.43	0.370	0.284	0.195
6.24	0.310	0.0501	0.029	6.51	0.325	0.225	0.174
6.39	0.303	0.0492	0.026	6.61	0.310	0.184	0.153
6.52	0.296	0.0483	0.022	6.69	0.300	0.144	0.133
6.64	0.289	0.0477	0.019	6.77	0.290	0.117	0.113
6.71	0.282	0.0471	0.016	6.83	0.289	0.0960	0.094
6.78	0.275	0.0467	0.012	6.86	0.281	0.0784	0.075
6.83	0.268	0.0464	0.009	6.89	0.274	0.0664	0.056
6.88	0.261	0.0461	0.006	6.91	0.264	0.0576	0.037
6.91	0.254	0.0460	0.003	6.93	0.254	0.0520	0.019
	System III				System for wide part of segment		
3.52	4.60	0.465	0.432	3.31	4.20	0.465	0.568
4.25	0.360	0.219	0.188	3.60	0.275	0.133	0.127
4.46	0.340	0.209	0.176	3.51	0.275	0.136	0.119
4.66	0.320	0.200	0.164	3.44	0.275	0.139	0.112
4.88	0.300	0.192	0.153	3.38	0.275	0.142	0.105
5.07	0.280	0.185	0.143	3.32	0.275	0.144	0.096
5.25	0.260	0.179	0.133	3.27	0.275	0.146	0.089
5.41	0.255	0.174	0.124	3.23	0.275	0.148	0.081
5.59	0.250	0.169	0.115	3.20	0.275	0.149	0.072
5.73	0.230	0.164	0.107	3.27	0.275	0.151	0.064
5.90	0.305	0.159	0.098	3.14	0.275	0.152	0.055
6.08	0.300	0.156	0.087	3.12	0.275	0.153	0.046
6.23	0.294	0.153	0.077	3.10	0.275	0.154	0.037
6.35	0.289	0.149	0.067	3.08	0.280	0.117	0.028
6.45	0.283	0.147	0.057	3.05	0.290	0.085	0.018
6.57	0.280	0.145	0.047	3.01	0.300	0.052	0.009
6.65	0.277	0.144	0.037				
6.71	0.274	0.113	0.028				
6.74	0.264	0.0826	0.019				
6.76	0.254	0.0520	0.009				

reactor. Some of these may be regarded as constraints, other as target values.

The upper limit on the pumping power fraction, K, is taken as 0.025, this being the maximum value for a gas-cooled fission reactor (Mitchell and Booth (19)) (it is also the value used by Shock (2)). For this value of K the design target wall loading quoted by Mitchell and Hollis (3) for a net (electrical) power output of 2000 MW is 6.7 MW/m^2. Shock (2) specified a minimum value of 4 MW/m^2. However, in a recent detailed review of the economics of fusion power generation, Hancox (20) finds that only for reactors with a net power output above 1000 MW need the wall loading be greater than 5 MW/m^2.

Establishing an upper bound on the structure fraction is less straightforward. In Sec. 2 it was stated that for systems I and II the structure fraction was 0.072 and depended solely on the dimensions of the cells. Although this value could possibly be reduced slightly by choosing a different arrangement for the cells, it can not fall below 0.0675, the value for a single cell of the recommended dimensions. On the other hand, the structure fraction for system III is a function of the cell and secondary feed pipe dimensions. Furthermore, since the wall thickness of the feed pipes increases with the coolant flow rate then so will the structure fraction. This variation is indicated on the curves relating to system III in the following figures.

In Fig. 8 the pumping power fraction/wall loading relations are shown for each of the three systems and it can be seen that system III exhibits the best performance characteristic. Even so, at the maximum value of pumping power fraction, 0.025, the wall loading is only 3.89 MW/m^2. Above this point the pumping power fraction increases rapidly and, in fact there is an asymptotic limiting value of wall loading of just over 5 MW/m^2, the reason for which is as follows. As the flow rate of coolant is increased the pressure drop across the flow circuit will obviously increase. At the same time the wall thickness of each pipe

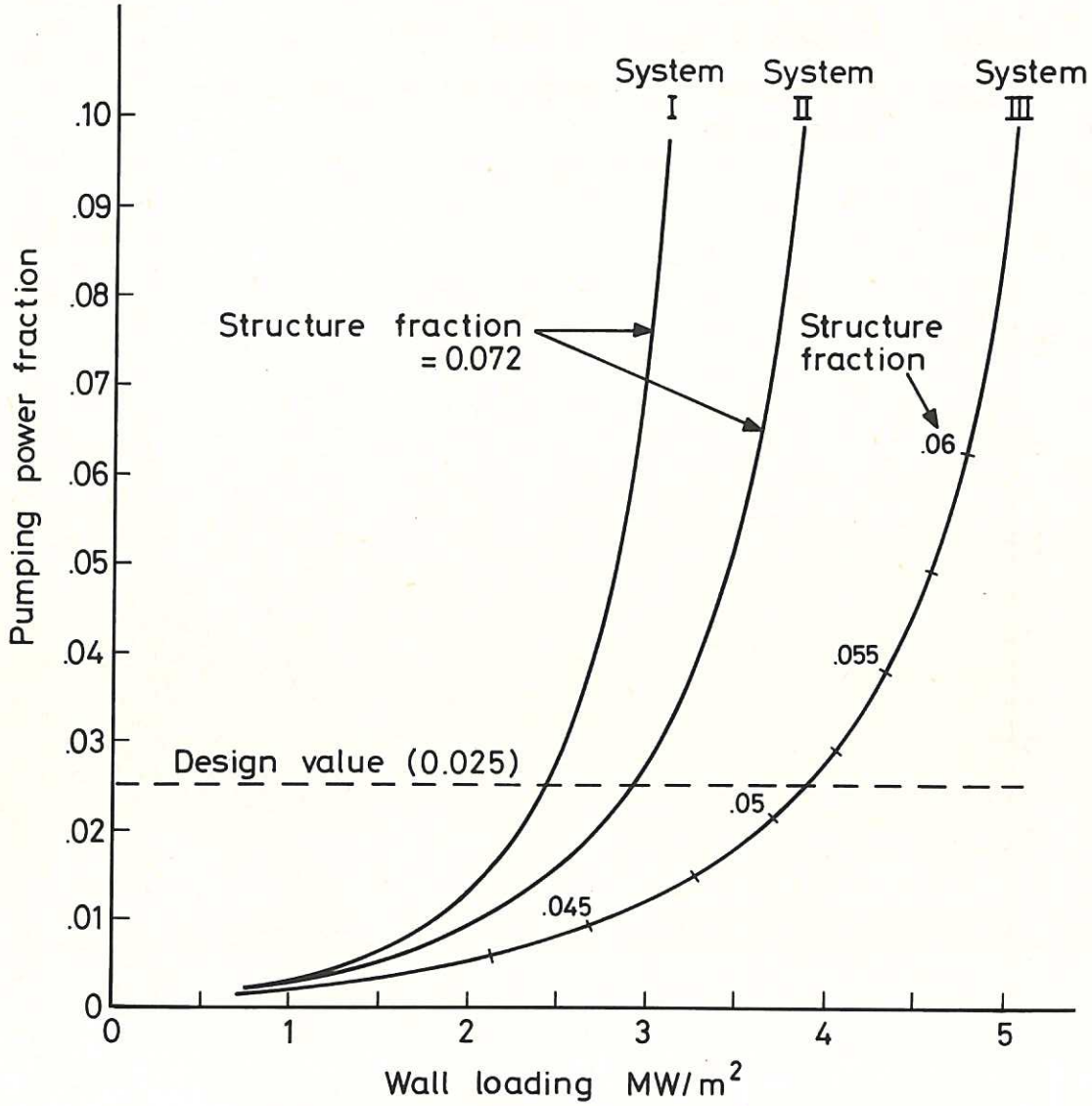

Fig.8 Performance curves for systems I, II, and III.

segment must increase and therefore, since the outside diameter is fixed, the bore must decrease. Eventually, a state is reached where the bore of the primary inlet feed pipe reaches zero and in consequence the pumping power becomes infinite. Just how the pressure drop across the circuit escalates is illustrated in Fig. 9 which shows how

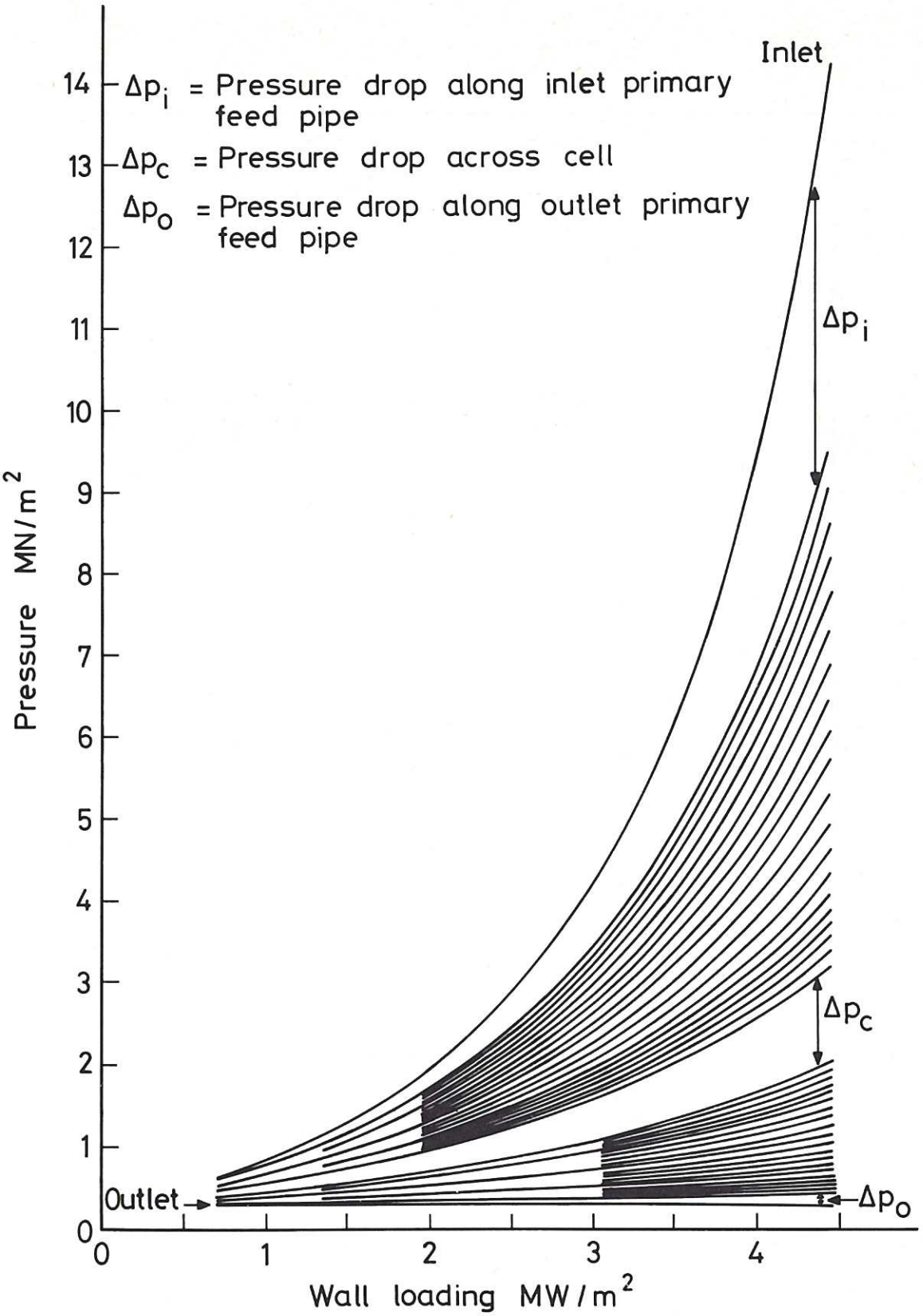

Fig.9 Cumulative variation of pressure drop along each pipe segment and cell with wall loading (system III).

the pressure at the end of each pipe segment varies with wall loading for system III.

Another favourable feature of system III is that its structure fraction at K = 0.025 is lower than that for systems I and II, being about 0.052. On the other hand, the outlet temperature of the lithium, and hence its temperature rise, is lower as can be seen from Fig. 10.

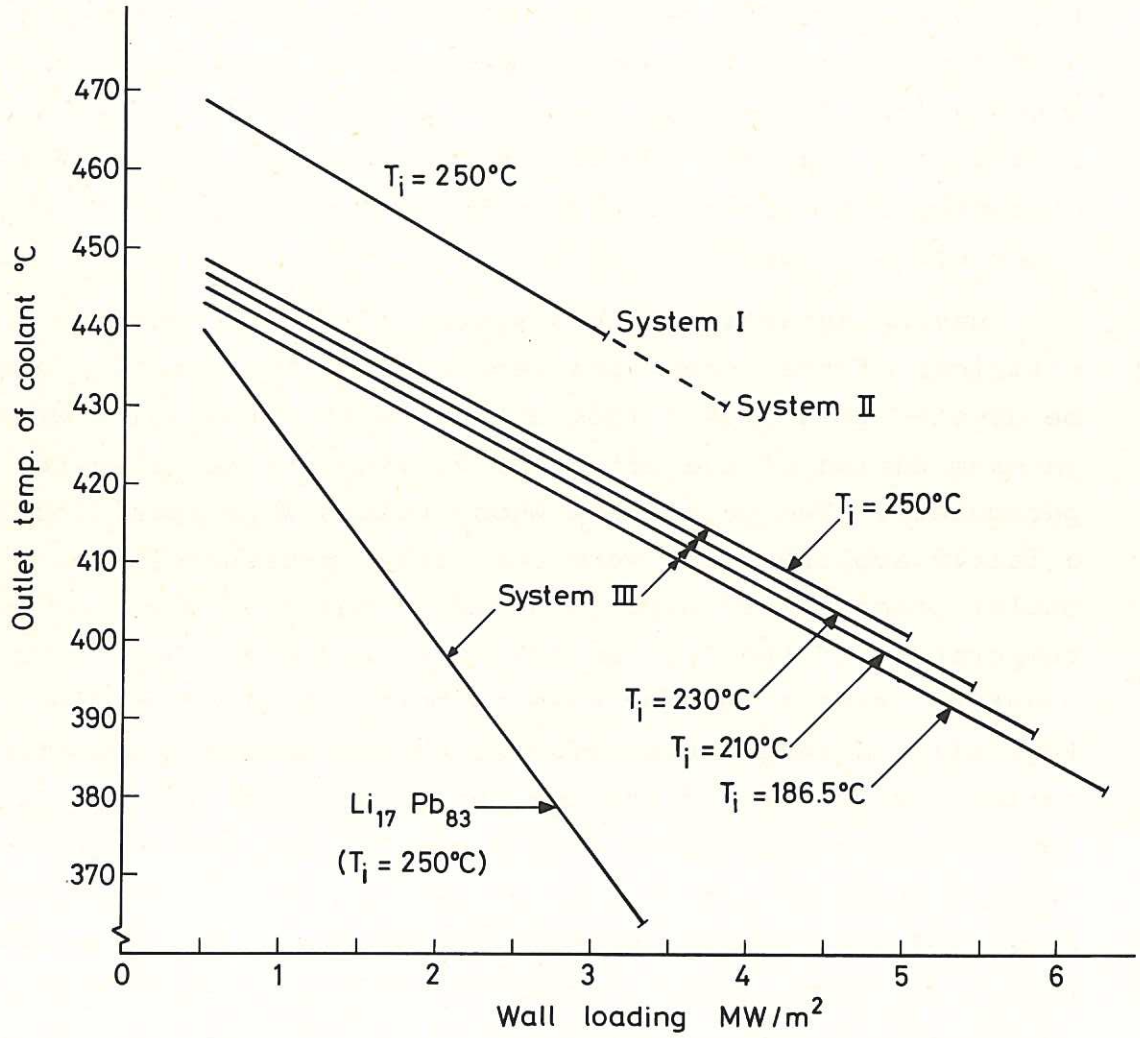

Fig.10 Variation of coolant outlet temperature with wall loading.

For system III the wall loading of 3.89 MW/m^2 is attained for a coolant flow rate of 0.335 kg/s to a cell on the innermost row which corresponds to a supply of 108 kg/s

to the whole half-segment. At entry to the cell the pressure is 2.45 MN/m^2 which, on using equation (3), leads to a wall thickness for the cell feed pipe of 0.53 mm and, hence, a conductance ratio of about 0.008. The distance between the end of this feed pipe and the front face of the cell is only 2.75 mm and the disturbed flow in the cell will extend for a distance of 0.275 m ($= a_f\Phi^{-\frac{1}{2}}$) or so behind its front face. On reaching the outlet of the cell the pressure has fallen to 1.6 MN/m^2 and so the value of Φ for the secondary feed pipe at this point is 0.005. Since $a\Phi^{-\frac{1}{2}} \sim 0.7$ m $\sim 5a_c$ it follows that the modifications to the pipe and cell dimensions of the last three cell rows of system III discussed in Sec 5.3 and illustrated in Fig. 6 are satisfactory.

Having established that system III is the most efficient of the three, the remainder of this section will be devoted to a closer look at that system beginning with an examination of the effect of varying the basic system parameters. Two parameters whose values were specified in a fairly arbitrary way were the outlet pressure in the outlet primary feed pipe (0.3 MN/m^2) and the inlet temperature of the lithium (250°C). Reducing the latter quantity leads to an increase in both wall loading (see Fig. 11) and temperature rise of the lithium although the outlet temperature of the coolant falls slightly (see Fig. 10). While the ultimate improvement is limited by the melting point of the lithium at 186°C, 210°C is possibly a more realistic minimum working temperature. Performance curves for these temperatures are shown in Fig. 11 and at the maximum pumping power fraction of 0.025 the improvement in wall loading is 22% for an inlet temperature of 210°C rising to 34% at 186°C. However, even now, the wall loading must be less than 5.22 MW/m^2.

The value of the outlet pressure must remain positive otherwise cavitation will occur but using a value of 0.3 MN/m^2 at low wall loadings, which of course signifies low flow rates, possibly yields pessimistic results while at high wall loadings the reverse is true. However, as shown

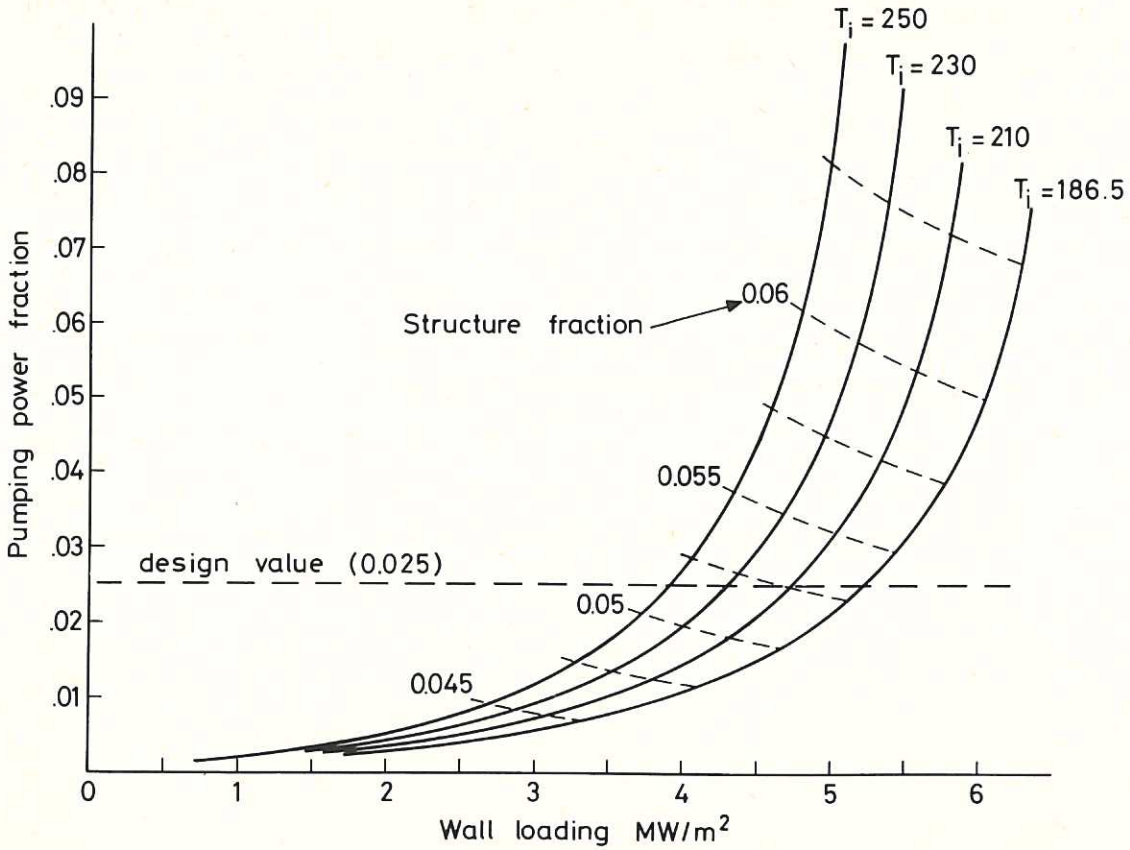

Fig.11 Effect of different lithium coolant inlet temperature on performance curve of system III.

in the curves for different outlet pressures in Fig. 12, at a pumping power fraction of 0.025, the wall loading can be increased by only 4% by decreasing the outlet pressure from 0.3 to 0.2 MW/m^2.

An inherent feature of the cells are the large temperature gradients that exist along them, typically of order 1000^{o}C/m (see Stanbridge et al (5, Table A1.2)). It has recently been recognised that such temperature gradients can be utilised to assist in driving the flow in the cell via the electric currents driven by the Seebeck effect interacting with the magnetic field (Shercliff (21)) and a possible way of incorporating such effects to advantage in

a reactor blanket has been examined by Dutta Gupta (22). These thermoelectric aspects of the flow will further complicate the analysis of the flow through the cell both from heat transfer and fluid mechanical points of view and at present it is only possible to assess their implications in qualitative terms. It would appear that positive pressure gradients can be set up that are of the same order as the negative ones known to exist in the cell, which would reduce the pressure drop across the cell. In Fig. 12 a curve has been calculated with the pressure drop across the cell set to zero, to give some idea of the improvement in wall loading that might be gained from this phenomenon.

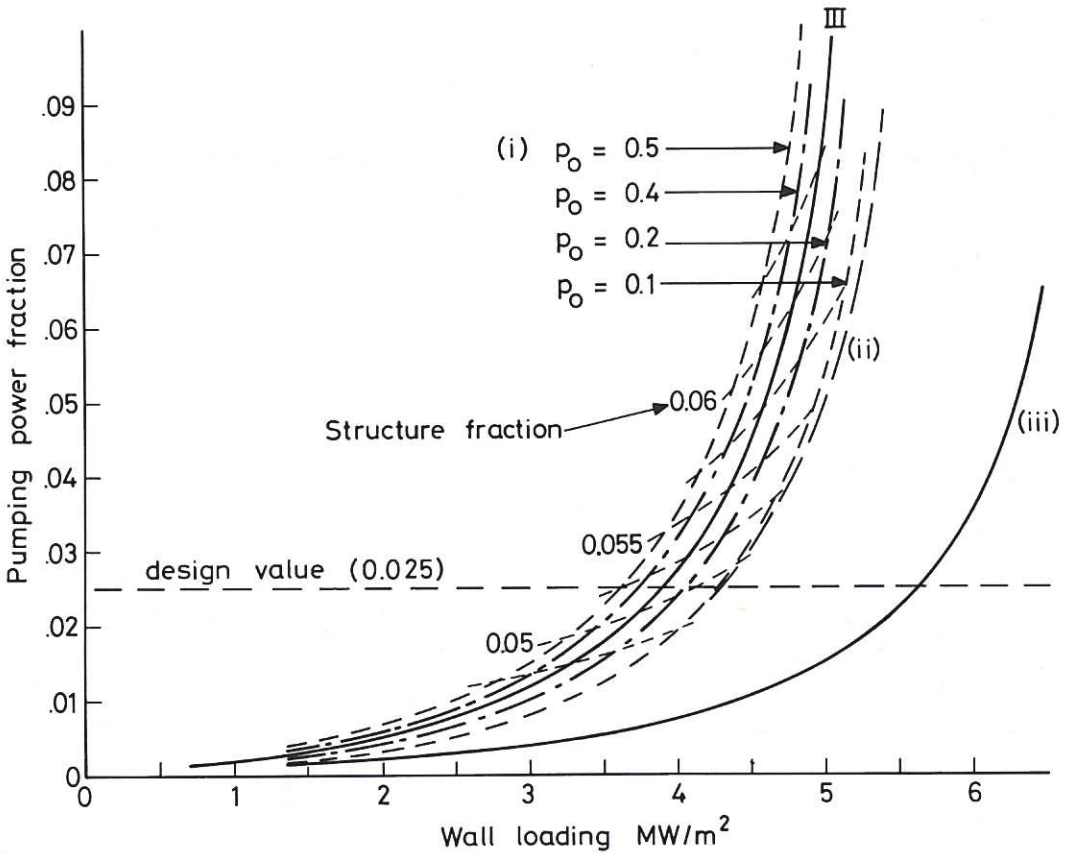

Fig.12 Effect of (i) different outlet pressures in primary feed pipe, (ii) zero cell pressure drop, (iii) zero pressure drop due to non-uniform magnetic fields and variable bore pipes (i.e. fully developed flow in all pipework) on performance curve of system III (Ti = 250° C).

Lowering the pressure drops associated with changes in pipe cross-section and/or magnetic field strength (equation (2)) will reduce the pumping power fraction. Neglecting these pressure drops corresponds to the case of fully-developed flow throughout the lithium coolant circuit except in the cell. The performance curve for this case is shown in Fig. 12 and indicates that neglecting these effects can lead to overestimating the possible wall loading by as much as 50% - i.e. an increase from 3.89 to 5.62 MW/m^2 at K = 0.025.

At this point, the principal conclusion that can be drawn from this study is that, for lithium coolant contained in stainless steel pipes and cells with one inlet and outlet primary feed pipe per half-segment it is not possible to achieve a wall loading of more than 5 MW/m^2 without excessive pumping power loss however the parameters of system III are varied. In the following paragraphs the effects of modifying system III, using different materials for the pipes and cells and using a different coolant will be examined.

First, Fig. 9 shows that for system III at 3.9 MW/m^2, about 25% of the total pressure drop arises from the flow in the primary feed pipe. This pressure drop can be reduced by dividing the flow to the half segment between two pairs of primary feed pipes - the first delivering 43% of the flow to the narrow side of the segment and the second supplying the wide part of the segment as described in section 5.4. The performance curves are shown in Fig. 13, separately for each part of the segment and added together to yield the performance of the modified system III. This indicates an improvement of 30% over the standard system III at K = 0.025 i.e. a wall loading of 5.05 MW/m^2.

Second, so far an all stainless steel system has been assumed - thus limiting the reactor performance (i.e. wall loading) by reason of the physical properties of the structure i.e. the steel itself. Equations (1), (2), and (3) (and those in section 3) show that the MHD pressure

drops vary directly with the pipe wall material conductivity. Equation (2) also shows that the wall thickness can be reduced given a higher working stress, with a further reduction in pressure drop from its dependence on wall thickness. Fig. 13 shows performance curves for a material which retains the properties of stainless steel except for either

(i) a 50% reduction of electrical conductivity
or (ii) an increase of working stress by a factor 2.

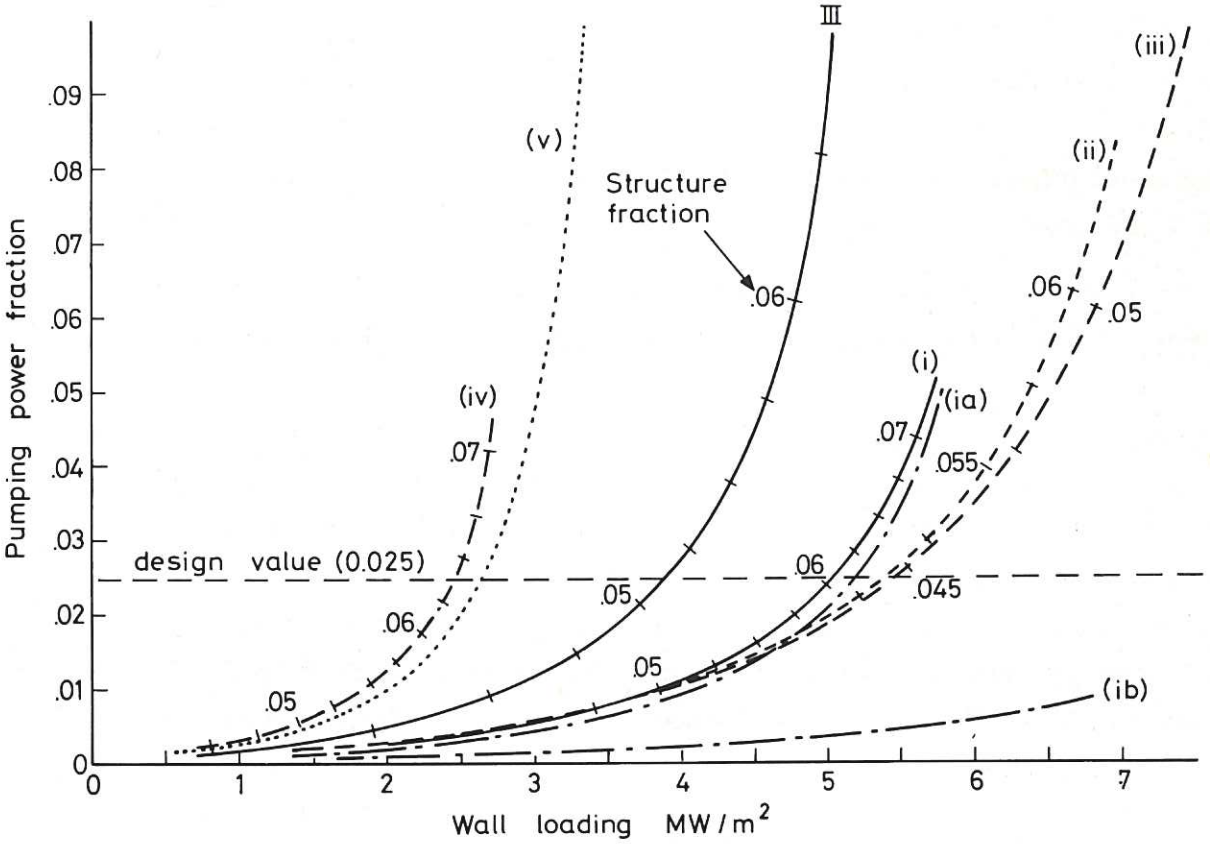

Fig.13 Effect of (i) feeding each side of half segment from separate primary feed pipe circuits (modified system III), (ii) reducing electrical conductivity of steel by 50%, (iii) increasing working stress of steel by 100% (iv) decreasing working stresses of steel by 50%, (v) using $Li_{17}Pb_{83}$ as coolant, on performance curve of system III. Performance curves for narrow (ia) and wide (ib) parts of segment supplied from their own primary feed pipes are shown.

While both changes show a similar potential improvement in wall loading of about 40% at K = 0.025, an increase in working stress could be more advantageous because of the reduction of structure fraction and potential for increased tritium breeding.

Equation (8) shows that the wall loading limit could be raised by increasing the permissible temperature in the flow circuit. However, even if the temperature limits imposed by creep and corrosion effect could be lifted, further improvement would be constrained by the fall off of working stress for stainless steel above 500°C (see Fig. 7 - working stress-fatigue limits).

So far the results have been based on working stress data for unirradiated stainless steel. In fact, due to the irradiaton environment and the possibility of pulsed operation of the reactor more severe stress limitations will be likely. To illustrate the significance of such effects a performance curve for a 50% decrease in the working stress of stainless steel has been added to Fig. 13. In this case, the wall loading at K = 0.025, 2.45 MW/m^2, represents a 37% reduction of the value for the basic system III, and is only slightly better than the value achieved by system I. However, this is a pessimistic viewpoint since in practice the irradiation damage to the structure will vary throughout the depth of the blanket.

Sze et al (23) have recently proposed the use of lithium-lead alloys as alternative coolants. The obvious attractions of such alloys are that they offer good tritium breeding and high neutron energy multiplication for a low lithium content. Against these points are their propensity to corrode steels although this does not appear to be an insoluble problem, particularly at temperatures of 500°C and below, and their greater density which would necessitate much stronger supporting structure.

$Li_{17}Pb_{83}$ is a eutectic alloy with the lowest melting point on the Li-Pb phase diagram being 235°C which would imply a minimum operating temperature of about 250°C. At

present there is only limited data on the properties of this material and the values used in the calculations here, together with their derivation, are given in Appendix III. When this alloy is substituted for lithium in the basic system III the resultant performance curve shown in Fig. 13 can be seen to be inferior to that for lithium coolant. In particular, for K = 0.025 the wall loading is only 2.63 MW/m^2, some 32% lower than the value for system III. Furthermore, Fig. 10 shows that the outlet temperature of this coolant is lower than that when lithium is the coolant and it decreases more rapidly as the wall loading increases.

Finally, it is worthwhile bearing in mind that some improvement in performance could be obtained by abandoning the symmetry of the inlet and outlet parts of the feed pipe systems. On the basis of Fig. 9 it will be appreciated that within certain limits, the advantage gained by using larger inlet feed pipes would outweigh the disadvantage of the necessarily smaller outlet feed pipes. However, optimisation of the feed pipe systems in this respect is not a straightforward matter and therefore has not been pursued here.

7. Conclusions

The principal constraints and limitations of this study are:-

(i) The symmetric inlet/outlet ducting and cellular blanket structure have been designed to fit the blanket segment of the Culham Conceptual Tokamak Reactor Mark IIA. Thus, to facilitate servicing and repair of blanket segments, this requires that there shall be a small number of jointed and accessible ducts between the segment proper and the external lithium circuit outside the reactor.

(ii) In the calculations of MHD pressure drop it is assumed that the lithium circuit is manufactured to

small dimensional tolerances and fine finishes on surfaces in contact with the lithium (e.g. the gap between the cell feed pipe and the inside nose of the cell must be maintained to within ~ ± 0.01 mm regardless of temperature changes during operation). The design of support structure for the blanket cells and ducting has not been considered. In some cases, the wall thickness is small:- e.g. the outlet primary feed duct for system III is almost 1m diameter, ~ 2mm wall thickness and contains about 300 kg lithium per metre of duct.

(iii) The working stress limits used for the duct design are for unirradiated stainless steel and are applied in the Lamé hoop stress formula. Allowing for compound and thermal stressing, the neutron irradiation environment and any fatigue of the structure will reduce the calculated wall loadings.

(iv) The analysis neglects the effects of erosion of the cell wall by the plasma and any variation of the wall loading due to system parameters - i.e. local variations in plasma energy and particle confinement. The mean reactor wall loadings would have to be lower than calculated and consequently the pumping power fraction would be greater than 2.5% of thermal output. Also since any fracture of the ducting or blanket cell itself would release lithium into the plasma and quench the fusion reaction, clearly there are serious doubts about performance reliability of this particular concept of a lithium cooled fusion reactor.

(v) It is assumed that the reactor has a high efficiency divertor which absorbs at least 66% of the α-particle energy. With a less efficient divertor the wall loading limits would be lower than those calculated here and some modification of the cell design might be required.

The results of this study are summarised in Table II, which gives the calculated wall loadings at a pumping power fraction of 0.025 and the percentage change compared with the system III model for all systems and for parameter variations in system III.

Thus assuming that it may be practical to operate at a lithium inlet temperature of 210°C (24°C above its melting point), and using one pair of primary ducts per half blanket segment, the calculated wall loading is 4.73 MW/m^2 - (line 2 of variations on system III).

System III (modified) shows a 30% improvement on the standard system III. Therefore if the additional complication of separate high and low pressure lithium circuits should be acceptable, the maximum wall loading could be raised to 1.3 x 4.73 = 6.15 MW/m^2.

Neglect of the pressure drops due to changing duct dimensions and magnetic fields gives results 44% high as indicated by assuming fully developed flow throughout system III. The advantage of a lower conductivity and/or a high strength alloy are also indicated in Table II by the calculations for double working stress and half electrical conductivity as compared with the standard system III.

While the calculated wall loadings given in Table II and above would have to be reduced to take account of irradiation damage for example it is not possible to assess the resulting constraint on system performance in the absence of the necessary materials data and information on plasma confinement.

Finally, whenever a liquid metal coolant is used, the reactor performance is limited ultimately by the fact that the ducting and (to a lesser extent) the cells are electrical conductors. If it ever became possible to use electrically non-conducting pipework, the performance would be radically improved because in the pressure drop equations (Sec 3) Φ is replaced by M^{-1} (Holroyd and Walker (7)) and so the pressure losses are much smaller since $M^{-1} << \Phi$ in a reactor.

Table II - Summary of results for lithium cooled Fusion Reactor Blanket design

Design Concept		Wall Loading at K = 0.025 MW/m^2	% increase on System III
System I	at standard conditions*	2.43	- 37
System II	"	2.92	- 25
System III	"	3.89	
System III (modified)	"	5.05	30
Variations on System III			
(1) Lithium Inlet Temperature T_i	= 230°C	4.30	10
(2) "	= 210°C	4.73	22
(3) "	= 186.5°C	5.22	34
(4) External circuit pressure drop p_o	= 0.5 MN/m^2	3.61	- 7
(5) "	= 0.4 MN/m^2	3.73	- 4
(6) "	= 0.2 MN/m^2	4.05	4
(7) "	= 0.1 MN/m^2	4.27	9
(8) Cell pressure drop Δp_c	= 0	4.29	10
(9) Fully developed flow throughout system		5.62	44
(10) Electrical conductivity of Stainless Steel	x 0.5	5.41	39
(11) Working stress of Stainless Steel	x 2.0	5.49	41
(12) "	x 0.5	2.45	- 37
(13) Lithium lead ($Li_{17}Pb_{83}$) coolant		2.63	- 32

* Standard conditions are defined as:

(i) all stainless steel structure with properties of unirradiated materials at constant strain shown in Fig. 7

(ii) steady state operation

(iii) maximum mean steel temperature of 475°C

(iv) lithium inlet temperature T_i = 250°C

(v) external circuit pressure drop p_o = 0.3 MN/m^2

Appendix I

At present for the simple lithium blanket considered here it is assumed that the total energy per fusion event is 20 MeV comprising

14.1 MeV to neutron fusion product
3.5 MeV to helium-ion (α-particle) fusion product
2.4 MeV from neutron reactions in the blanket

In previous estimates the third item in this list was taken as 4.8 MeV; this lower figure accounts for the fact that some of the reactions are endothermic. Thus, the wall loadings and lithium energy input rates shown by Stanbridge et al (5, Fig. A1) must be reduced by factors of

$$(14.1 + 3.5 + 2.4)/(14.1 + 3.5 + 4.8) = 20/22.4$$

and $$(14.1 + 2.4)/(14.1 + 4.8) = 16.5/18.9$$

respectively. A revised version of that graph is shown in Fig. 4.

Appendix II

The value of the temperature rise along the inlet secondary feed pipes depends upon the layout of pipes, reflector and supporting structure and so here only an estimate of its magnitude can be made. In the calculations the curve shown in Fig. 4 is represented by the fitted curve -

$$q_{Li}(x) = 5.156\ e^{-x/0.184} + 1.223\ e^{-(L'-x)/0.184}$$

where x is the distance measured from the front of the cell and L' is the position of the front face of the reflector. The energy input to a pipe segment is taken as the product of the pipe segment length and the integral of $q_{Li}(x)$ over the cross-section of that pipe whose diameter is assumed to fill the complete available space (in the pressure loss calculations these pipe diameters are smaller by a factor of 0.8). In the integration the value of L' varies over the rear half of the pipe. This process eventually yields a temperature rise of $0.00618\ P_w/c_p Q\ ^oC$ for system III and $0.00955\ P_w/c_p Q\ ^oC$ for the system feeding the wide part of the segment described in Sec. 5.4.

Appendix III

From the graphs presented by Sze et al (23) the following properties of $Li_{17}Pb_{83}$ may be deduced.

(i) Density = $9495 - 0.695 \times (T - 235)$ kg/m^3

where T is the temperature in degrees centigrade.

(ii) Values for the electrical conductivity of the solid alloy at 50, 100 and 150°C and the liquid alloy at 800°C are given. The former three values define a straight line which can be extrapolated to give a value at 235°C. By comparing this value and that at 800°C with the values for the constituent metals over that range the following result may be derived, namely

$$\text{conductivity} = 10^8/(22.06 + 0.166 \times T) \quad S$$

for $250^{\circ}C < T < 475^{\circ}C$.

There appear to be no values for the specific heat and thermal conductivity of the alloy available. However, a value for the former can be estimated from the values of the parent metals and the Kopp-Neumann law as 170 J/kg °C at 360°C. On the basis of a comparison between the relative magnitudes of the thermal conductivities of sodium, potassium and sodium-potassium alloys a value of 21 W/m °C has been used for the thermal conductivity of $Li_{17}Pb_{83}$. While this value is open to argument it should be noted that it does not significantly affect the results.

Notation

a	tube radius
a_c	radius of cell body
a_f	radius of inlet feed pipe in cell
A_c	representative cross sectional area of cell = $2\sqrt{3}\ a_c^2$
B	magnetic field strength
c_p	specific heat of coolant
f	working stress (of stainless steel)
k	thermal conductivity
K	pumping power fraction
ℓ	length of tube segment
L	length of cell body
L_a	length of annulus formed by reflector in cell
L'	distance of front face of reflector from front of cell
M	Hartmann number = $aB\sqrt{\sigma/\eta}$
N	interaction parameter = $M^2/R_e = \pi\sigma a^3 B^2/Q$
p	pressure
Δp	pressure drop
δp	pressure drop component in cell
P_w	wall loading
q	energy input rate per unit wall loading
Q	local mass flow rate of coolant
R_e	Reynolds number = $Q/\pi\eta a$
t	wall thickness
t_c	wall thickness of cell
t_f	distance between end of cell feed pipe and end of cell
T	temperature
ΔT	temperature rise
x	distance co-ordinate from front of cell
β	fraction of P_w which directly raises coolant temperature
Φ	conductance ratio = $\sigma_w t/\sigma a$
σ	electrical conductivity of coolant
σ_w	electrical conductivity of stainless steel wall
ρ	density of coolant
η	viscosity of coolant

References

1. HUNT, J.C.R., HANCOX, R. The use of liquid lithium as coolant in a toroidal fusion reactor. Pt I Calculation of pumping power. UKAEA Res. Group Rep., Culham Laboratory, CLM-R115, 1971

2. SHOCK, R.A.W. Helium cooling circuits for a fusion reactor. Nuclear Engineering and Design 61:277, 1980

3. MITCHELL, J.T.D., HOLLIS, A A tokamak reactor with servicing capability. Proc. 9th Symp. Fusion. Tech. Pergamon Press, 1976

4. MITCHELL, J.T.D., HANCOX, R. A lithium cooled toroidal fusion reactor. Proc. Intersoc. Energy Conversion Eng. Conf., San Diego, USA, 1972

5. STANBRIDGE, J.R., CARRUTHERS, H.M., KEEN, B.A., SHOTTER, H.A. Design of stainless steel blanket cells for a fusion reactor. UKAEA Res. Group Rep., Culham Laboratory, CLM-R127, 1974

6. HUNT, J.C.R., HOLROYD, R.J. Applications of laboratory and theoretical MHD duct flow studies in fusion reactor technology. UKAEA Res. Group. Rep., Culham Laboratory CLM-R169, 1977

7. HOLROYD R.J., WALKER, J.S. A theoretical study of the effects of wall conductivity, non-uniform magnetic fields and variable area ducts on liquid metal flows at high Hartmann number. J. Fluid. Mech. 84:471, 1978

8. HOLROYD, R.J. An experimental study of the effects of wall conductivity, non-uniform magnetic fields and variable area ducts on liquid metal flows at high Hartmann number. Pt II Ducts with conducting walls. J. Fluid Mech. 96:355, 1980

9. HOLROYD, R.J. MHD duct flows in non-uniform magnetic fields. Ph.D. Dissertation, University of Cambridge, 1976

10. CHANG, C.C., LUNDGREN, T.S. Duct flow in MHD. Z. angew. Math. Phys. 12:100, 1961

11. HOLROYD, R.J., HUNT, J.C.R. Theoretical and experimental studies of liquid metal flows in strong non-uniform, magnetic fields in ducts with complex geometry. Proc. 2nd Bat-Sheva Int. Sem. on MHD flows and turbulence. Israel Univ. Press, 1980

12. CARRUTHERS, H.M. Structural design of demountable blanket elements and shield for a fusion reactor. UKAEA Res. Group Rep., Culham Lab., CLM-R151, 1976

13. ROGERS, G.F.C., MAYHEW, Y.R. Engineering thermodynamic work and heat transfer. Longmans, 1965 (7th impression)

14. MITCHELL, J.T.D. Blanket replacement in toroidal fusion reactors, Proc. 3rd ANS Topical Meeting on the Technology of Controlled Nuclear Fusion, Santa Fe, May 1978

15. BRIARS, D.A., STANBRIDGE, J.R. Design of the segment structure and coolant ducts for a fusion reactor blanket and shield. UKAEA Res. Group. Rep., Culham Lab., CLM-R184, 1978

16. BRIARS, D.A., STANBRIDGE, J.R. The feasibility of remotely separating and rejoining the main coolant pipes of a fusion reactor. UKAEA Res. Group Rep., Culham Laboratory, CLM-R174, 1977

17. MANSTELLER, J.W., TEPPER, S., RODGERS, F.J. Alkali metals handling and systems operating techniques. Gordon and Breach, 1967

18. KAYE, G.W.C., LABY, T.H. Tables of physical and chemical constants and some mathematical functions. Longmans, 1973 (14th edition)

19. MITCHELL, J.T.D., BOOTH, J.A. Wall loading limitations in a helium cooled fusion reactor blanket. UKAEA Res. Group Rep., Culham Laboratory, CLM-R126, 1973

20. HANCOX, R. Factors affecting the minimum capital cost of a Tokamak reactor. Proc. 11th Symp. Fusion Tech., Oxford, Pergamon Press, 1980

21. SHERCLIFF, J.A. Thermoelectric MHD in fusion technology. Proc. 11th Symp. Fusion. Tech., Oxford. Pergamon Press, 1980

22. DUTTA GUPTA, P.B. A conceptual composite blanket design for the tokamak type of thermonuclear reactor incorporating thermoelectric pumping of liquid lithium. Proc. 11th Symp. Fusion Tech., Oxford. Pergamon Press, 1980

23. SZE, D.K., CLEMMER, R., CHENG, E.T. LiPb, a novel material for fusion applications. Proc. 4th ANS Topical Meeting on the Technology of Controlled Nuclear Fusion, King of Prussia, PA., Oct 1980

HER MAJESTY'S STATIONERY OFFICE

Government Bookshops

49 High Holborn, London WC1V 6HB
(London post orders: PO Box 569, London SC1 9NH)
13a Castle Street, Edinburgh EH2 3AR
41 The Hayes, Cardiff CF1 1JW
Brazennose Street, Manchester M60 8AS
Southey House, Wine Street, Bristol BS1 2BQ
258 Broad Street, Birmingham B1 2HE
80 Chichester Street, Belfast BT1 4JY

Publications may also be ordered through any bookseller